Spectroscopic and Excited-State Properties of Luminescent Rhenium(I) N-Heterocyclic Carbene Complexes Containing Aromatic Diimine Ligands

ARTICLE *in* ORGANOMETALLICS · MARCH 1998

Impact Factor: 4.13 · DOI: 10.1021/om9709042

Spectroscopic and Excited-State Properties of Luminescent Rhenium(I) N-Heterocyclic Carbene Complexes Containing Aromatic Diimine Ligands

Wen-Mei Xue, Michael Chi-Wang Chan, Zhong-Min Su, Kung-Kai Cheung, Shiuh-Tzung Liu,† and Chi-Ming Che*

Department of Chemistry, The University of Hong Kong, Pokfulam Road, Hong Kong

Received October 16, 1997

Rhenium(I) N-heterocyclic carbene complexes of the type $[HNCH_2CH_2NHCRe(L-L)(CO)_3]^+$ have been prepared, where L−L = 4,4′-dimethoxy-2,2′-bipyridine (**2**), 4,4′-bis(*tert*-butyl)-2,2′-bipyridine (**3**), 2,2′-bipyridine (**4**), 4,4′-dichloro-2,2′-bipyridine (**5**), 4,4′-bis(carbomethoxy)-2,2′-bipyridine (**6**), 5-phenyl-1,10-phenanthroline (**7**), and *o*-phenylenebis(diphenylphosphine) (**8**). The molecular structures of **4**, **6**, and **8** have been determined by X-ray analyses and show Re−C(carbene) bond distances of 2.171(7), 2.163(4), and 2.199(6) Å, respectively. HF-SCF and MP_2 calculations on the model compound $[HNCH_2CH_2NHCRe(NHCHCHNH)(CO)_3]^+$ (**4m**) show that the HOMO is nonbonding d(Re) and the LUMO is mainly π^*(diimine) with partial p_z(carbene) character. CIS calculations on the excited state of optimized **4m** suggest that the lowest energy absorption originates from a HOMO to LUMO spin-forbidden transition. Complexes **2**−**7** are emissive at room temperature and 77 K. The room-temperature and 77 K luminescence data of **2**−**6** are consistent with emission from a ^{3}-MLCT state. The nature of the emission of **7** at room temperature is also ^{3}MLCT but changes to IL at 77 K. Complex **8** does not emit at room temperature, but at 77 K, the IL π(pdpp) → π^*(pdpp) emission is observed. The combination of detailed spectroscopic studies and theoretical calculations reveal that the emitting state at room temperature is ^{3}[d(Re) → π^*-(diimine)], with the latter exhibiting partial σ^*(carbene) parentage. The excited-state energies and redox potentials can be tuned using diimine ligands with varying electron-donating/accepting abilities.

Introduction

Studies on transition-metal carbene complexes have given prominence to their stoichiometric and catalytic reactivities and to their important roles in a number of organic transformations.[1] In contrast, little attention has been devoted to their photophysical and -chemical properties,[2] even though photolysis might be expected to alter the reactivity of the carbene ligand through population of charge-transfer excited states. The photochemistry of pentacarbonyltungsten and -chromium carbene complexes have been extensively studied.[3] Geoffroy and co-workers reported that the photolysis of $W(CO)_5\{C(OMe)Ph\}$ resulted in CO elimination as the only detectable photoreaction.[2a] This reaction was proposed to proceed via ligand-field excited states with the lowest lying W → π^*(carbene) charge-transfer state being inactive with respect to CO loss. A large body of work describing the photochemistry of chromium carbene complexes has been reported by Hegedus and co-workers.[4]

To gain insight into the photochemical reactions of carbene complexes, it is necessary to characterize the lowest-lying electronic excited states and their photophysical deactivation mechanisms. Emission spectroscopy often provides a highly sensitive and effective way to identify and study the lowest-energy excited states,[5] but the first example of a *luminescent* carbene complex has only appeared recently.[6]

† Department of Chemistry, National Taiwan University, Taipei, Taiwan.

(1) Dötz, K. H.; Fischer, H.; Hofmann, P.; Kreissl, F. R.; Schubert, U.; Weiss, K. *Transition Metal Carbene Complexes*; Verlag Chemie: Weinheim, Germany, 1983.

(2) (a) Foley, H. C.; Strubinger, L. M.; Targos, T. S.; Geoffroy, G. L. *J. Am. Chem. Soc.* **1983**, *105*, 3064. (b) Bell, S. E. J.; Gordon, K. C.; McGarvey, J. J. *J. Am. Chem. Soc.* **1988**, *110*, 3107. (c) Rooney, A. D.; McGarvey, J. J.; Gordon, K. C.; McNicholl, R. A.; Schubert, U.; Hepp, W. *Organometallics* **1993**, *12*, 1277. (d) Rooney, A. D.; McGarvey, J. J.; Gordon, K. C. *Organometallics* **1995**, *14*, 107. (e) For recent review, see: Hegedus, L. S. *Comprehensive Organometallic Chemistry* II.; Abel, E. W., Stone, F. G. A., Wilkinson, G., Eds., Pergamon: Oxford, 1995; Vol. 12, p 549.

(3) (a) Fischer, E. O.; Fischer, H. *Chem. Ber.* **1974**, *107*, 657. (b) Casey, C. P.; Shusterman, A. J. *J. Mol. Catal.* **1970**, *8*, 1. (c) Casey, C. P.; Shusterman, A. J.; Vollendorf, N. W.; Haller, K. J. *J. Am. Chem. Soc.* **1982**, *104*, 2417. (d) Dahlgren, R. M.; Zink, J. I. *Inorg. Chem.* **1977**, *16*, 3154. (e) Edwards, B. H.; Rausch, M. D. *J. Organomet. Chem.* **1981**, *210*, 91.

(4) (a) McGuire, M. A.; Hegedus, L. S. *J. Am. Chem. Soc.* **1982**, *104*, 5538. (b) Hegedus, L. S.; McGuire, M. A.; Schultze, L. M.; Yujin, C.; Anderson, O. P. *J. Am. Chem. Soc.* **1984**, *106*, 2680. (c) Borel, C.; Hegedus, L. S.; Krebs, J.; Satoh, Y. *J. Am. Chem. Soc.* **1987**, *109*, 1101. (d) Hegedus, L. S.; deWeck, G.; D'Andrea, S. *J. Am. Chem. Soc.* **1988**, *110*, 2122. (e) Lastra, E.; Hegedus, L. S. *J. Am. Chem. Soc.* **1993**, *115*, 87. (f) Hegedus, L. S. *Acc. Chem. Res.* **1995**, *28*, 299. (g) Hegedus, L. S. *Tetrahedron* **1997**, *53*, 4105.

(5) Lees, A. J. *Chem. Rev.* **1987**, *87*, 711.

(6) Lai, S. W.; Chan, M. C. W.; Cheung, K. K.; Che, C. M. *Angew. Chem., Int. Ed. Engl.* **1998**, *37*, 182.

S0276-7333(97)00904-7 CCC: $15.00
Publication on Web 03/25/1998

Scheme 1

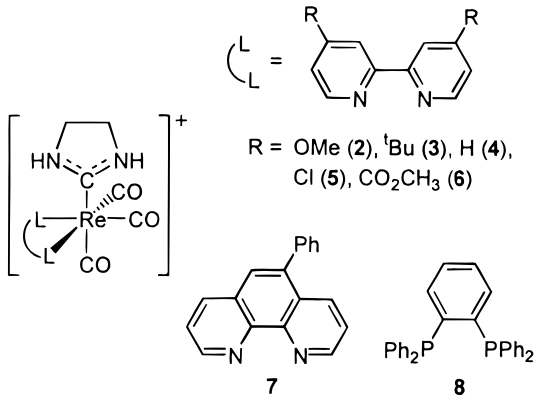

We now report on the luminescence of rhenium(I) N-heterocyclic carbene derivatives with diimine or phosphine ligands, as depicted in Scheme 1. Some of the molecular structures are determined by X-ray crystal analyses. Assignment of the lowest-lying excited state is based on photophysical studies and molecular orbital calculations, and subtle tuning of the excited-state energies and redox potentials is also demonstrated.

Experimental Section

General Procedures. $Re(CO)_5Cl$ (Strem), 2,2′-bipyridine (bpy, Aldrich), 5-phenyl-1,10-phenanthroline (Phphen, GFS), and *o*-phenylenebis(diphenylphosphine) (pdpp, Strem) were used as received. 4,4′-Dimethoxy-2,2′-bipyridine ($(MeO)_2$-bpy),[7] 4,4′-bis(*tert*-butyl)-2,2′-bipyridine ($^tBu_2$-bpy),[8] 4,4′-dichloro-2,2′-bipyridine (Cl_2-bpy),[9] 4,4′-bis(carbomethoxy)-2,2′-bipyridine ($(MeO_2C)_2$-bpy),[9] and $Br(CO)_4Re\overline{CNHCH_2CH_2NH}$ (**1**)[10] were prepared by literature methods. The dichloromethane for the photophysical studies was washed with concentrated sulfuric acid, 10% sodium hydrogen carbonate, and water, dried by calcium chloride, and distilled over calcium hydride. The acetonitrile for the photophysics and electrochemistry was distilled over potassium permanganate and calcium hydride. The other solvents used were of analytical grade.

Infrared spectra were recorded with KBr disks on a BIO-RAD FTS165 FT-IR spectrophotometer. Fast atom bombardment (FAB) mass spectra were obtained on a Finnigan Mat 95 mass spectrometer. Elemental analyses were performed by Butterworth Laboratory, U.K. ^1H, ^{13}C, and ^{31}P NMR measurements were performed on a JEOL 270, Bruker DRX 300, or 500 MHz FT-NMR spectrometer with TMS (^1H and ^{13}C) and H_3PO_4 (^{31}P) as the internal reference. UV−vis absorption spectra were obtained on a Milton Roy Spectronic 3000 diode-array spectrophotometer.

Cyclic voltammetry was performed with a Princeton Applied Research (PAR) model 175 universal programmer and a model 273 potentiostat. A standard two-compartment cell was used with glassy carbon as the working electrode, $Ag-AgNO_3$ (0.1 mol dm^{-3} in acetonitrile) as the reference electrode, and platinum wire as the counter electrode. The supporting electrolyte was *n*-tetrabutylammonium hexafluorophosphate (0.1mol dm^{-3}). $Cp_2Fe^{+/0}$ was added as an internal standard.

Emission and Lifetime Measurements. Steady-state emission spectra were recorded on a SPEX 1681 FLOURO-LOG-2 series F111AI spectrophotometer. Low- temperature (77 K) emission spectra for glasses and solid-state samples were recorded in 5-mm diameter quartz tubes which were placed in a liquid nitrogen Dewar equipped with quartz windows. The emission spectra were corrected for monochromator and photomultiplier efficiency and for xenon lamp stability.

The absolute emission quantum yield was measured by the method of Demas and Crosby[11] using quinine sulfate in 0.1 N sulfuric acid as the standard. Sample and standard solutions were degassed with at least three freeze−pump−thaw cycles. The quantum yield of the sample was determined by

$$\Phi_s = \Phi_r(B_r/B_s)(n_s/n_r)^2(D_s/D_r)$$

where the subscripts s and r refer to sample and reference standard solution, respectively; n is the refractive index of the solvents; D is the integrated intensity, and Φ is the luminescence quantum yield. The quantity B is calculated by

$$B = 1-10^{-AL}$$

where A is the absorbance at the excitation wavelength and L is the optical path length.

Emission lifetimes and flash-photolysis measurements were performed with a Quanta Ray DCR-3 pulsed Nd:YAG laser system (pulse output 355 nm, 8 ns). The emission signals were detected by a Hamamatsu R928 photomultiplier tube and recorded on a Tektronix model 2430 digital oscilloscope.

Syntheses. $[\overline{HNCH_2CH_2NHC}Re(L-L)(CO)_3]^+$ (L−L = 4,4′-X_2-bpy, X = OMe (2), ^{t}Bu (3), H (4), Cl (5), CO_2Me (6)). Complex **1** (0.10 g, 0.23 mmol) and L−L (0.27 mmol) in benzene (10 cm^3) were refluxed for 4 h to give a yellow or orange precipitate. Upon cooling, the resultant solid was collected and washed with benzene and diethyl ether. Recrystallization by diffusion of diethyl ether into an acetonitrile solution afforded crystals of the complexes $[\overline{HNCH_2CH_2NHC}Re(L-L)(CO)_3]Br$. The perchlorate salt was prepared by metathesis of the bromide salt in methanol using lithium perchlorate, and crystals were obtained by diffusion of diethyl ether into an acetonitrile solution.

2: Yellow crystals of the ClO_4^- salt, yield 0.12 g, 79%. IR (ν_{CO}, cm^{-1}): 2022, 1924, 1895. MS (positive FAB): *m*/*z* 557 (M^+), 529 (M^+ − CO). Anal. Calcd for $C_{18}H_{18}N_4O_9ClRe$: C, 32.96; H, 2.77; N, 8.54. Found: C, 32.66; H, 2.78; N, 8.20. ^1H NMR (CD_3CN): δ 3.30 (s, 4, CH_2), 4.08 (s, 6, CH_3O), 6.80 (s, br, 2, NH), 7.20 (dd, 2, J_{HH} = 6.5, 2.7 Hz, py H), 8.03 (d, 2, J_{HH} = 2.7 Hz, py H), 8.83 (d, 2, J_{HH} = 6.5 Hz, py H). ^{13}C NMR (CD_3CN): δ 45.2 (CH_2), 58.1 (CH_3O), 112.2, 115.0, 155.8, 158.3, 169.3 (py C), 194.2 (carbene C), 197.6 (ax-CO), 201.6 (eq-CO).

3: Yellow crystals of the ClO_4^- salt, yield 0.14 g, 86%. IR (ν_{CO}, cm^{-1}): 2033, 1924, 1903. MS (positive FAB): *m*/*z* 609 (M^+), 581 (M^+ − CO). Anal. Calcd for $C_{24}H_{30}N_4O_7ClRe$: C, 40.70; H, 4.27; N, 7.91. Found: C, 40.92; H, 4.52; N, 8.15. ^1H NMR (CD_3CN): δ 1.46 (s, 18, CH_3), 3.30 (s, 4, CH_2), 6.63 (s, br, 2, NH), 7.67 (dd, 2, J_{HH} = 1.9, 5.9 Hz, py H), 8.43 (d, 2, J_{HH} = 1.9 Hz, py H), 8.91 (d, 2, J_{HH} = 5.9 Hz, py H). ^{13}C NMR (CD_3CN): δ 30.5 (CH_3), 36.7 (CMe_3), 45.3 (CH_2), 122.8, 126.2, 154.3, 156.6, 165.9 (py C), 193.7 (carbene C), 197.6 (ax-CO), 201.1 (eq-CO).

4: Yellow crystals of the Br^- salt, yield 0.11 g, 83%. IR (ν_{CO}, cm^{-1}): 2022, 1936, 1905. MS (positive FAB): *m*/*z* 497 (M^+), 469 (M^+ − CO). Anal. Calcd for $C_{16}H_{14}N_4O_3BrRe$: C, 33.34; H, 2.45; N, 9.72. Found: C, 33.12; H, 2.53; N, 10.01. ^1H NMR (CD_3CN): δ 3.28 (s, 4, CH_2), 6.80 (s, br, 2, NH), 7.68 (m, 2, py

(7) Maerker, G.; Case, F. H. *J. Am. Chem. Soc.* **1958**, *80*, 2745.
(8) Chen, T. Y. Ph.D. Thesis, National Taiwan University, 1993.
(9) Cook, M. J.; Lewis, A. P.; McAnliffe, G. S. G.; Skarda, V.; Thomson, A. J.; Glasper, J. L.; Robbins, D. J. *J. Chem. Soc., Perkin Trans. II* **1984**, 1293.
(10) Liu, C. Y.; Chen, D. Y.; Lee, G. H.; Peng, S. M.; Liu, S. T. *Organometallics* **1996**, *15*, 1055.
(11) Demas, J. N.; Crosby, G. A. *J. Phys. Chem.* **1971**, *75*, 991.

H), 8.23 (td, 2, $J_{HH,t}$ = 8.0 Hz, $J_{HH,d}$ = 1.5 Hz, py H), 8.51 (d, 2, J_{HH} = 8.0 Hz, py H), 9.09 (m, 2, py H). ^{13}C NMR (CD_3CN): δ 45.2 (CH_2), 125.5, 129.2, 140.9, 154.9, 156.6 (py C), 193.5 (carbene C), 197.4 (ax-CO), 200.8 (eq-CO).

5: Yellow crystals of the ClO_4^- salt, yield 0.12 g, 78%. IR (ν_{CO}, cm^{-1}): 2028, 1941, 1891. MS (positive FAB): *m/z* 565 (M^+), 537 ($M^+ - CO$). Anal. Calcd for $C_{16}H_{12}N_4O_7Cl_3Re$: C, 28.90; H, 1.82; N, 8.43. Found: C, 28.52; H, 1.74; N, 8.81. ^{1}H NMR (CD_3CN): δ 3.29 (s, 4, CH_2), 6.71 (s, br, 2, NH), 7.74 (dd, 2, J_{HH} = 6.0, 2.2 Hz, py H), 8.60 (s, 2, py H), 8.98 (d, 2, J_{HH} = 6.0 Hz, py H). ^{13}C NMR (CD_3CN): δ 45.2 (CH_2), 126.5, 129.6, 148.7, 155.7, 157.2 (py C), 192.9 (carbene C), 197.0 (ax-CO), 200.2 (eq-CO).

6: Orange crystals of the ClO_4^- salt, yield 0.13 g, 79%. IR (ν_{CO}, cm^{-1}): 2031, 1941, 1909. MS (positive FAB): *m/z* 613 (M^+), 585 ($M^+ - CO$). Anal. Calcd for $C_{20}H_{18}N_4O_{11}ClRe$: C, 33.71; H, 2.55; N, 7.87. Found: C, 33.71; H, 2.38; N, 7.73. ^{1}H NMR (CD_3CN): δ 3.26 (s, 4, CH_2), 4.04 (s, 6, CH_3), 6.53 (s, br, 2, NH), 8.11 (dd, 2, J_{HH} = 5.6, 1.4 Hz, py H), 8.97 (d, 2, J_{HH} = 1.4 Hz, py H), 9.21 (d, 2, J_{HH} = 5.6 Hz, py H). ^{13}C NMR (CD_3CN): δ 45.3 (CH_2), 54.2 (CH_3), 125.0, 128.3, 141.8, 155.8, 157.3 (py C), 164.8 (CO_2), 192.5 (carbene C), 197.0 (ax-CO), 199.9 (eq-CO).

[HNCH$_2$CH$_2$NHCRe(Phphen)(CO)$_3$]ClO$_4$ (7). A mixture of **1** (0.10 g, 0.23 mmol) and Phphen (0.07 g, 0.27 mmol) in benzene (10 mL) was heated to reflux for 6 h. The resultant orange solution was evaporated to dryness, and the residue was dissolved in CH_2Cl_2 (5 mL). Diethyl ether was added to precipitate the bromide salt. The yellow crystalline perchlorate salt was obtained as for complexes **2**−**6**: yield 0.13 g, 81%. IR (ν_{CO}, cm^{-1}): 2023, 1909 (br). MS (positive FAB): *m/z* 597 (M^+), 569 ($M^+ - CO$). Anal. Calcd for $C_{24}H_{18}N_4O_7ClRe$: C, 41.41; H, 2.61; N, 8.05. Found: C, 41.32; H, 2.36; N, 7.92. ^{1}H NMR (CD_3CN): δ 3.19 (s, 4, CH_2), 6.98 (s, br, 2, NH), 7.62 (m, 5, aryl H), 7.99 (dq, 2, $J_{HH,d}$ = 13.9 Hz, $J_{HH,q}$ = 5.2 Hz, aryl H), 8.16 (s, 1, aryl H), 8.64 (dd, 1, J_{HH} = 8.6, 1.3 Hz, aryl H), 8.80 (dd, 1, J_{HH} = 7.7, 1.3 Hz, aryl H), 9.53 (qd, 2, $J_{HH,q}$ = 5.2 Hz, $J_{HH,d}$ = 1.3 Hz, aryl H). ^{13}C NMR (CD_3CN): δ 45.1 (CH_2), 127.5, 128.0, 128.5, 129.9, 130.1, 131.0, 131.5, 137.9, 138.5, 139.9, 141.5, 146.9, 147.9, 155.5 (aryl C), 193.5 (carbene C), 197.4 (ax-CO), 200.6 (eq-CO).

[HNCH$_2$CH$_2$NHCRe(pdpp)(CO)$_3$]Br (8). A benzene solution (10 mL) of **1** (0.10 g, 0.23 mmol) and pdpp (0.12 g, 0.27 mmol) was refluxed for 4 h to give a white precipitate. Upon cooling to room temperature, the solid was collected and washed with benzene and diethyl ether. Recrystallization by diffusion of diethyl ether into an acetonitrile solution afforded colorless crystals: yield 0.16 g, 78%. IR (ν_{CO}, cm^{-1}): 2031, 1958, 1931. MS (positive FAB): *m/z* 787 (M^+), 759 ($M^+ - CO$). Anal. Calcd for $C_{36}H_{30}N_2O_3BrP_2Re$: C, 49.89; H, 3.49; N, 3.23. Found: C, 50.22; H, 3.41; N, 3.47. ^{1}H NMR (CD_3CN): δ 3.13 (s, 4, CH_2), 6.33 (s, 2, NH), 7.16 (m, 4, aryl H), 7.38 (m, 6, aryl H), 7.46 (m, 4, aryl H), 7.56 (m, 6, aryl H), 7.83 (m, 2, aryl H), 7.90 (m, 2, aryl H). ^{13}C NMR (CD_3CN): δ 45.9 (CH_2), 129.3−141.2 (m, aryl C), 189.9 (t, $^2J_{CP}$ = 9.7 Hz, carbene C), 191.5 (t, $^2J_{CP}$ = 6.6 Hz, ax-CO), 192.2 (d, $^2J_{CP}$ = 8.7 Hz, eq-CO), 192.5 (d, $^2J_{CP}$ = 8.6 Hz, eq-CO). ^{31}P NMR (CD_3CN): δ 37.6.

X-ray Crystallography. Crystals of [HNCH$_2$CH$_2$NHCRe(bpy)(CO)$_3$]Br·CH_3CN·0.5H_2O (**4**), [HNCH$_2$CH$_2$NHCRe(4,4′-$(CO_2Me)_2$-bpy)(CO)$_3$]ClO_4·H_2O (**6**), and [HNCH$_2$CH$_2$NHCRe(pdpp)(CO)$_3$]Br (**8**) were mounted on a Rigaku AFC7R diffractometer at 301 K with graphite-monochromated Mo Kα radiation (λ = 0.710 73 Å) using $\omega-2\theta$ scans at a scan speed of 16.0°/min and $2\theta_{max}$ = 50°. Intensity data were corrected for decay and Lorentz and polarization effects, and empirical absorption corrections were made based on the ψ-scan of six strong reflections. The structures were solved by direct methods (SIR92[13] for **4**) or by Patterson methods (for **6** and **8**), expanded by Fourier methods (PATTY[14]), and refined by full-matrix least-squares using the software package TeXsan on a Silicon Graphics Indy computer.

For complex **4**, two Br atoms and the O atoms of the water molecule were at special positions with an occupation number of $^1/_2$. All 30 non-H atoms were refined anisotropically. The hydrogen atoms of the water molecule were not located. Seventeen H atoms were included in the calculation, and these comprised of two H atoms bonded to the N(3) and N(4) atoms located in the difference Fourier synthesis and 15 H atoms at calculated positions with thermal parameters equal to 1.3 times that of the attached C atoms, but their positional parameters were not refined.

For complex **6**, all 38 non-H atoms were refined anisotropically. The two H atoms bonded to the N(3) and N(4) atoms were located in the difference Fourier synthesis, and their positional parameters were refined. The hydrogen atoms of the water molecule were not located. The other 16 H atoms at calculated positions with thermal parameters equal to 1.3 times that of the attached C atoms were not refined.

For complex **8**, all 45 non-H atoms were refined anisotropically. The two H atoms bonded to the N(1) and N(2) atoms were located in the difference Fourier synthesis, and their positional parameters were refined. The hydrogen atoms of the water molecule were not located. The other 28 H atoms at calculated positions with thermal parameters equal to 1.3 times that of the attached C atoms were not refined.

The crystal data are summarized in Table 1, and selected bond distances and angles are listed in Table 2.

Hartree−Fock Self-Consistent-Field and Second-Order Moller−Plesset Calculations. HF-SCF[15] and MP_2[16] calculations have been performed using the GAUSSIAN 94/DFT program package[17] on a Silicon Graphics Indigo 2 workstation. For the Re atom, the quasirelativistic (QR) pseudopotential (pp) developed by Hay and Wadt[18] with 15 valence electrons (VE) and the LANL2DZ basis sets associated with the pseudopotential were adopted. The basis sets were taken as Re[8s6p3d]/(3s3p2d), N[10s5p]/(3s2p), O[10s5p]/(3s2p), C[10s5p]/(3s2p), and H[4s]/(2s). The geometry of the calculation molecule [HNCH$_2$CH$_2$NHCRe(NHCHCHNH)(CO)$_3$]$^+$-(**4m**) was adapted from the X-ray structure of **4**.

Results and Discussion

Characterization and Crystal Structures. The carbene complexes **2**−**7** are stable both in the solid and

(12) Freni, M.; Giusto, D.; Romiti, P. *J. Inorg. Nucl. Chem.* **1967**, *29*, 761.

(13) Altomare, A.; Cascarano, M.; Giacovazzo, C.; Guagliardi, A.; Burla, M. C.; Polidori, G.; Camalli, M. *J. Appl. Crystallogr.* **1994**, *27*, 435.

(14) Beurskens, P. T.; Admiraal, G.; Beurskens, G.; Bosman, W. P.; Garcia-Granda, S.; Gould, R. O.; Smits, J. M. M.; Smykalla, C. *The DIRDIF program system*. Technical Report of the Crystallography Laboratory; University of Nijmegen: The Netherlands, 1992.

(15) (a) Roothan, C. C. J. *Rev. Mod. Phys.* **1951**, *23*, 69. (b) Pople, J. A.; Nesbet, R. K. *J. Chem. Phys.* **1959**, *22*, 571. (c) McWeeny, R.; Dierksen, G. *J. Chem. Phys.* **1968**, *49*, 4852.

(16) (a) Head-Gorden, M.; Pople, J. A.; Frisch, M. J. *Chem. Phys. Lett.* **1988**, *153*, 503. (b) Frisch, M. J.; Head-Gorden, M.; Pople, J. A. *Chem. Phys. Lett.* **1990**, *166*, 275. (c) Frisch, M. J.; Head-Gorden, M.; Pople, J. A. *Chem. Phys. Lett.* **1990**, *166*, 281.

(17) Frisch, M. J.; Trucks, G. W.; Schlegel, H. B.; Gill, P. M. W.; Johnson, B. G.; Robb, M. A.; Cheeseman, J. R.; Keith, T.; Petersson, G. A.; Montgomery, J. A.; Raghavachari, K.; Al-Laham, M. A.; Zakrzewski, V. G.; Ortiz, J. V.; Foresman, J. B.; Cioslowski, J.; Stefanov, B. B.; Nanayakkara, A.; Challacombe, M.; Peng, C. Y.; Ayala, P. Y.; Chen, W.; Wong, M. W.; Andres, J. L.; Replogle, E. S.; Gomperts, R.; Martin, R. L.; Fox, D. J.; Binkley, J. S.; Defrees, D. J.; Baker, J.; Stewart, J. P.; Head-Gordon, M.; Gonzalez, C.; Pople, J. A. *Gaussian 94, Revision C.3*; Gaussian, Inc.: Pittsburgh, PA, 1995.

(18) (a) Hay, P. J.; Wadt, W. R. *J. Chem. Phys.* **1985**, *82*, 270. (b) Schwerdtfeger, P.; Dolg, M.; Schwarz, W. H. E.; Bowmaker, G. A.; Boyd, P. D. W. *J. Chem. Phys.* **1989**, *91*, 1762.

Table 1. Crystal Data for Complexes 4, 6, and 8

	4	**6**	**8**
formula	$C_{18}H_{18}BrN_5O_{3.5}Re$	$C_{20}H_{20}ClN_4O_{12}Re$	$C_{36}H_{30}BrN_2O_3P_2Re$
fw	626.49	730.07	866.71
color	pale yellow	yellow	colorless
cryst dimens, mm	0.25 × 0.20 × 0.30	0.20 × 0.20 × 0.35	0.15 × 0.05 × 0.20
cryst syst	orthorhombic	triclinic	triclinic
space group	*Ccca* (No. 68)	$P\bar{1}$ (No. 2)	$P\bar{1}$ (No. 2)
a, Å	19.512(8)	11.826(6)	12.027(8)
b, Å	29.865(8)	12.012(6)	16.75(1)
c, Å	14.523(8)	11.694(5)	9.582(3)
α, deg		117.45(3)	105.26(4)
β, deg		97.33(4)	109.93(4)
γ, deg		60.61(3)	73.23(5)
V, Å^3	8462(5)	1274(1)	1708(1)
Z	16	2	2
ρ_{calcd}, g cm^{-3}	1.967	1.903	1.685
abs coeff, cm^{-1}	76.71	49.45	48.62
no. of unique data collected	4088	4485	6008
no. of obsd data with $I \geq 3\sigma(I)$	2584	4036	4776
no. of variables	259	349	412
R^a	0.028	0.023	0.030
$R_w{}^b$	0.039	0.026	0.034
goodness-of-fit, S^c	1.89	1.45	1.25
$\Delta\rho$(max, min, e Å^{-3})	+1.13, −0.67	+0.62, −0.54	+0.80, −1.01

^{a} $R = \sum(||F_o| - |F_c||)/\sum|F_o|$. ^{b} $R_w = [\sum w(|F_o| - |F_c|)^2/\sum w|F_o|^2]^{1/2}$. ^{c} $S = [\sum w(|F_o| - |F_c|)^2/(n - p)]^{1/2}$.

Table 2. Selected Bond Distances (Å) and Angles (deg) for Complexes 4, 6, and 8

		Complex **4**	
Re(1)−N(1)	2.178(6)	Re(1)−N(2)	2.175(6)
Re(1)−C(1)	1.917(9)	Re(1)−C(2)	1.924(9)
Re(1)−C(3)	1.965(9)	Re(1)−C(4)	2.171(7)
C(4)−N(3)	1.33(1)	C(4)−N(4)	1.32(1)
N(1)−Re(1)−N(2)	74.0(2)	N(1)−Re(1)−C(1)	173.2(3)
N(1)−Re(1)−C(2)	97.6(3)	N(1)−Re(1)−C(3)	92.7(2)
N(1)−Re(1)−C(4)	87.5(2)	N(2)−Re(1)−C(1)	99.2(3)
N(2)−Re(1)−C(2)	171.0(3)	N(2)−Re(1)−C(3)	93.2(3)
N(2)−Re(1)−C(4)	85.5(2)	C(1)−Re(1)−C(2)	89.1(4)
C(1)−Re(1)−C(3)	88.4(3)	C(1)−Re(1)−C(4)	91.2(3)
C(2)−Re(1)−C(3)	90.5(3)	C(2)−Re(1)−C(4)	90.9(3)
C(3)−Re(1)−C(4)	178.6(3)	Re(1)−C(4)−N(3)	125.1(5)
Re(1)−C(4)−N(4)	126.7(5)	N(3)−C(4)−N(4)	108.2(6)
		Complex **6**	
Re(1)−N(1)	2.178(3)	Re(1)−N(2)	2.172(3)
Re(1)−C(1)	1.908(5)	Re(1)−C(2)	1.928(5)
Re(1)−C(3)	1.966(5)	Re(1)−C(4)	2.163(4)
C(4)−N(3)	1.321(5)	C(4)−N(4)	1.318(5)
N(1)−Re(1)−N(2)	75.0(1)	N(1)−Re(1)−C(1)	171.3(2)
N(1)−Re(1)−C(2)	98.4(2)	N(1)−Re(1)−C(3)	94.5(2)
N(1)−Re(1)−C(4)	83.5(1)	N(2)−Re(1)−C(1)	97.7(2)
N(2)−Re(1)−C(2)	173.2(1)	N(2)−Re(1)−C(3)	91.9(2)
N(2)−Re(1)−C(4)	87.5(1)	C(1)−Re(1)−C(2)	88.8(2)
C(1)−Re(1)−C(3)	90.5(2)	C(1)−Re(1)−C(4)	91.5(2)
C(2)−Re(1)−C(3)	90.1(2)	C(2)−Re(1)−C(4)	90.3(2)
C(3)−Re(1)−C(4)	178.0(2)	Re(1)−C(4)−N(3)	127.1(3)
Re(1)−C(4)−N(4)	126.2(3)	N(3)−C(4)−N(4)	106.7(4)
		Complex **8**	
Re(1)−P(1)	2.437(1)	Re(1)−P(2)	2.444(1)
Re(1)−C(1)	1.963(6)	Re(1)−C(2)	1.950(6)
Re(1)−C(3)	1.928(7)	Re(1)−C(4)	2.199(6)
C(4)−N(1)	1.328(7)	C(4)−N(2)	1.318(7)
P(1)−Re(1)−P(2)	82.57(5)	P(1)−Re(1)−C(1)	175.5(2)
P(1)−Re(1)−C(2)	92.7(2)	P(1)−Re(1)−C(3)	94.1(2)
P(1)−Re(1)−C(4)	89.1(2)	P(2)−Re(1)−C(1)	93.3(2)
P(2)−Re(1)−C(2)	175.1(2)	P(2)−Re(1)−C(3)	93.9(2)
P(2)−Re(1)−C(4)	89.5(2)	C(1)−Re(1)−C(2)	91.4(2)
C(1)−Re(1)−C(3)	87.9(2)	C(1)−Re(1)−C(4)	89.1(2)
C(2)−Re(1)−C(3)	87.7(2)	C(2)−Re(1)−C(4)	89.1(2)
C(3)−Re(1)−C(4)	175.6(2)	Re(1)−C(4)−N(1)	129.3(4)
Re(1)−C(4)−N(2)	122.8(4)	N(1)−C(4)−N(2)	107.9(5)

solution state. Their infrared spectra show a pattern of three peaks in the carbonyl region (2022−2031, 1924−1941, and 1891−1909 cm^{-1}) which are typical for *fac*-Re(L−L)(CO)$_3$X complexes. In the ^{13}C NMR spectra, the resonances for the carbene carbon appear in the 189.9−194.2 ppm range, which is comparable to that of 192.0 ppm in complex **1**.[10]

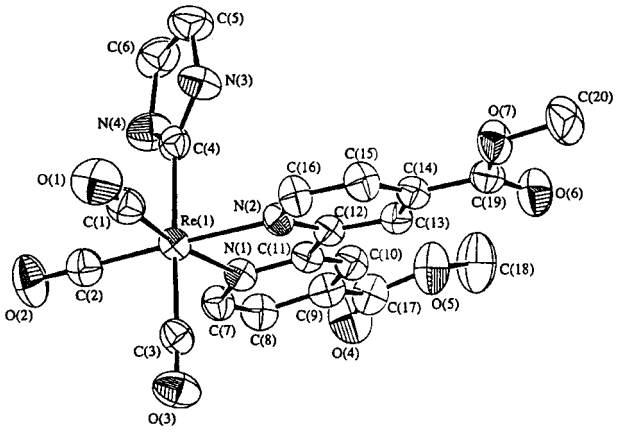

Figure 1. ORTEP plot of the cation in complex **6** (40% probability ellipsoids).

The molecular structures of **4** (see Supporting Information), **6**, and **8** (Figures 1 and 2, respectively) have been determined by X-ray diffraction methods. The rhenium atom in each case has a pseudo-octahedral geometry (Table 2) with the three carbonyl ligands in a facial configuration and the carbene group trans to one of these (C(3)−Re(1)−C(4) 178.6(3)°, 178.0(2)°, and 175.6(2)° for **4**, **6**, and **8**, respectively). The Re−C(carbene)−N angles approach 120°, in agreement with sp^2 hybridization at the carbene carbon atoms (e.g., in complex **8**, Re(1)−C(4)−N(1) 129.3(4)°, Re(1)−C(4)−N(2) 122.8(4)°, N(1)−C(4)−N(2) 107.9(5)°).

Previous studies revealed that the metal−carbene bond distances are perturbed by the organic substituents attached to the carbene carbon.[1] In this work, the Re−C(carbene) distances (2.171(7), 2.163(4), and 2.199(6) Å for **4**, **6**, and **8**, respectively) are comparable with those in other heteroatom-stabilized analogues such as *fac*-ReBr(CO)$_3$(CNHCH$_2$CH$_2$NH)$_2$ (2.14(2) and 2.17(2)

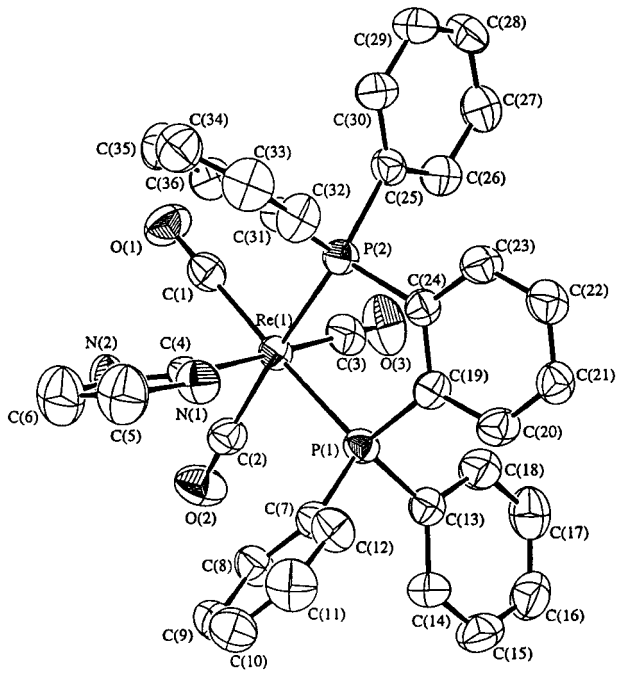

Figure 2. ORTEP plot of the cation in complex **8** (40% probability ellipsoids).

Å),[10] ReBr(CO)$_4$(COCH$_2$CH$_2$O) (2.135(13) Å),[19] ReBr(CO)$_4${C(NHPh)(NHCHMe$_2$)} (2.206(10) Å),[20] and ReBr(CO)$_3$(PPh$_3$){C(NHPh)(NHCHMe$_2$)} (2.215(8) Å).[20] They are longer than the Re−alkylcarbene contact in CpRe(NO)(PPh$_3$)(CHPh)$^+$ (1.949(6) Å)[21] but are similar to the Re−C(sp^3) bond in the corresponding benzyl derivative CpRe(NO)(PPh$_3$)(CH$_2$Ph)$^+$ (2.203(8) Å).[22] Nevertheless, the angles around the carbene atoms in **4**, **6**, and **8** imply that there are appreciable Re−C(carbene) π interactions in these complexes.

Electronic Structure and Absorption Spectra. As an aid to interpreting the electronic absorption spectra of complexes **2**−**7**, HF-SCF[15] and MP$_2$[16] calculations have been performed on the model molecule [HNCH$_2$CH$_2$NHCRe(NHCHCHNH)(CO)$_3$]$^+$ (**4m**). The calculated energy and composition of the near frontier orbitals are summarized in Table 3 and reveal that the HOMO has a high d(Re) parentage (69.5%) whereas the LUMO is dominated by π*(diimine) (78.3%) and the percentage of p(carbene C) is small (6.5%). Figure 3 shows a simplified molecular orbital diagram of **4m** and its component fragments [(CO)$_3$Re(NHCHCHNH)]$^+$ and CNHCH$_2$CH$_2$NH. The HOMO is essentially the nonbonding d$_{xz}$(Re) orbital, and below this are the two nonbonding d$_{yz}$(Re) and d$_{x^2-y^2}$(Re) orbitals (x, y, z axis defined as in Figure 3); these three orbitals are very close in energy. The LUMO is comprised of p$_z$(diimine) and p$_z$(carbene C). Hence, if the lowest energy transition involves the frontier orbitals (see Supporting Information), then this is formulated as d(Re) → π*(diimine) mixed with a small amount of d(Re) → σ*(carbene C).

Table 3. Calculated Energy (eV) and Composition (%) of the Near Frontier Orbitals of Model Molecule [HNCH$_2$CH$_2$NHCRe(NHCHCHNH)(CO)$_3$]$^+$ (4m) by MP$_2$ Method

		% composition				
orbital	energy, eV	Re	carbene C	HNCH$_2$-CH$_2$NH	3CO	NHCH-CHNH
72	1.265	14.9	5.4	4.6	64.2	11.0
71	0.972	35.2	3.3	9.8	31.3	20.4
70	0.883	39.4	12.5	10.4	22.8	14.9
69	0.465	3.7	0.7	2.4	9.1	84.1
68	0.177	56.6	11.0	5.5	18.6	8.4
67	0.020	51.9	1.0	2.1	32.3	12.8
66	−0.265	73.6	6.5	8.2	6.7	5.0
65	−0.696	66.0	1.7	2.6	9.6	20.2
64	−1.192	69.2	1.9	4.0	11.3	13.6
63	−3.996	6.5	6.5	1.1	7.6	78.3
62	−12.245	69.5	0.3	1.7	19.2	9.2
61	−12.357	68.1	1.1	3.5	18.7	8.7
60	−12.584	73.5	0.2	0.1	23.5	2.7
59	−14.244	0.6	0.8	97.1	0.7	0.8
58	−15.959	8.6	47.3	19.6	13.1	11.4
57	−16.208	5.4	8.9	6.1	4.1	75.4
56	−17.848	1.7	10.2	59.3	4.5	24.3
55	−18.077	5.5	0.1	1.3	19.7	73.4
54	−18.245	2.2	2.7	66.2	7.0	21.9
53	−18.448	4.4	4.0	26.8	9.7	55.1
52	−18.993	4.0	5.6	15.4	8.3	66.7
51	−19.821	1.4	0.7	7.4	89.1	1.5
50	−19.873	1.7	0.1	4.0	90.7	3.5
49	−20.016	0.5	0.2	75.7	22.9	0.7
48	−20.030	1.8	0.3	16.2	78.6	3.1
47	−20.265	1.9	1.5	63.0	29.2	4.4
46	−20.500	5.3	0.2	0.2	86.5	7.8
45	−20.565	3.9	0.3	20.3	71.1	4.4
44	−20.710	5.0	0.5	7.5	83.5	3.5
43	−20.915	10.1	0.6	3.4	81.1	4.9

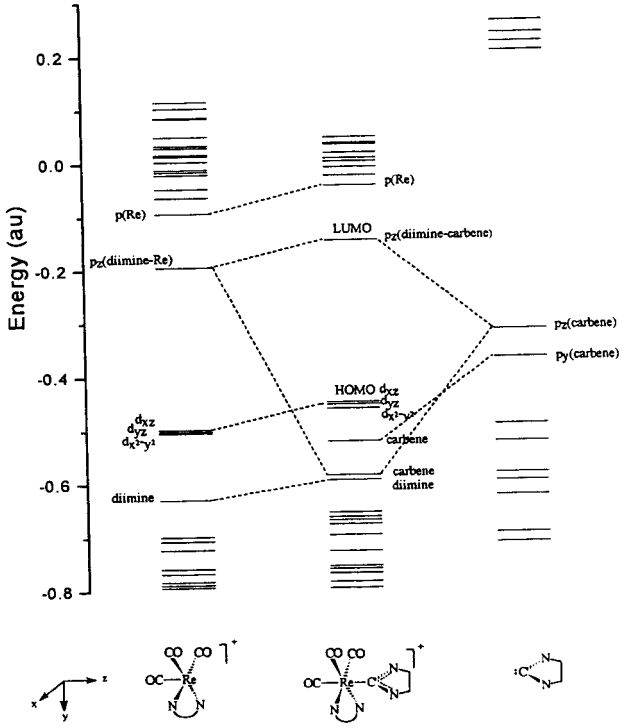

Figure 3. Simplified orbital mixing diagram for **4m**. Orbital energies are derived from MP$_2$ calculation.

The electronic absorption spectral data of complexes **1**−**8** are summarized in Table 4. We suggest that

(19) Miessler, G. L.; Kim, S.; Jacobson, R. A.; Angelici, R. J. *Inorg. Chem.* **1987**, *26*, 1690.
(20) Chen, L. C.; Chen, M. Y.; Chen, J. H.; Wen, Y. S.; Lu, K. L. *J. Organomet. Chem.* **1992**, *425*, 99.
(21) Kiel, W. A.; Lin, G. Y.; Constable, A. G.; McCormick, F. B.; Strouse, C. E.; Eisenstein, O.; Gladysz, J. A. *J. Am. Chem. Soc.* **1982**, *104*, 4865.
(22) Merrifield, J. H.; Strouse, C. E.; Gladysz, J. A. *Organometallics* **1982**, *1*, 1204.

Table 4. UV−Vis Absorption Spectral Data of Complexes 1−8 in Dichloromethane and Acetonitrile at Room Temperature

	CH_2Cl_2		CH_3CN	
complex	λ, nm[a]	ϵ, 10^3 dm^3 mol^{-1} cm^{-1} [b]	λ, nm[a]	ϵ, 10^3 dm^3 mol^{-1} cm^{-1} [b]
1	346 tail to 560	3.0		
	308	7.4		
2	350 tail to 490	4.9	342	5.8
	294	14.6	294	15.9
	277	23.2	252	47.8
	255	36.9		
3	355 tail to 500	4.5	345	4.7
	315	9.6	314	9.2
	267	20.0	250	21.4
	253	20.7		
4	365 tail to 510	3.5	355	4.2
	318	8.0	316	11.1
	273	15.4	245	25.5
5	380 tail to 530	3.7	375	4.3
	283	15.5	278	21.1
	255	14.0	253	23.6
6	400 tail to 570	6.2	390	6.1
	305	21.9	300	21.5
7	370 tail to 510	4.0	360	4.7
	320	6.7	320	8.3
	286	18.2	283	24.5
8	350	0.02		
	300	2.2		

[a] Error = ±2 nm. [b] Error = ±1 in the last digit.

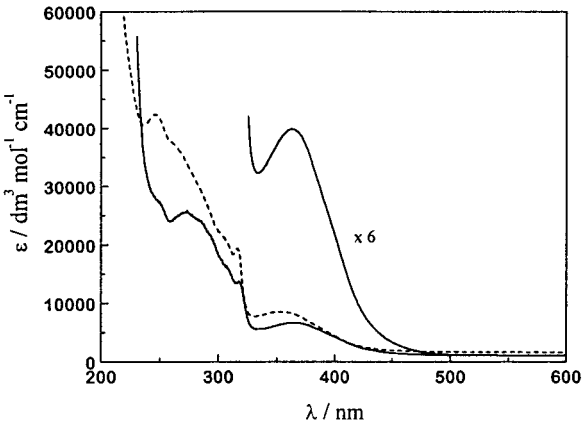

Figure 4. UV−vis absorption spectra of **4** in dichloromethane (—) and acetonitrile (- - -) at room temperature.

complex **1** has a similar electronic structure to that of $W[C(OMe)Ph](CO)_5$;[2a] thus, the moderately intense band centered at 346 nm in the UV−vis absorption spectrum of **1** is assigned as the spin-allowed d(Re) → π*(carbene C) (MLCT) transition, while the very weak shoulder tailing to 560 nm is assigned as a spin-forbidden d(Re) → π*(carbene C) (^{3}MLCT) transition. Replacing the CO ligands by diimine evidently affects the electronic structure of the carbene complexes (*vide supra*). The UV−vis absorption spectrum for complex **4** is shown in Figure 4.

To aid in the interpretation of the absorption spectra of these rhenium(I) carbene complexes, a single configuration interaction (CIS) calculation[23] was performed on the excited state of the optimized molecule **4m**, where all the orbitals and electrons of the ground state were included to take into account the electronic correlation for the excited states. The results and assignments are listed in Table 5. The calculated lowest energy absorption at 433 nm is a triplet transition of orbital 62 → 63 (HOMO to LUMO). This can be visualized as a spin-forbidden charge-transfer transition of d_{xz}(Re) to π*-(diimine), where the π*(diimine) orbital has a small percentage of p_z(carbene C), and is denoted as ^{3}MLCT. From the absorption spectrum of **4**, a weak shoulder around 450 nm correlates with this transition. The calculated HOMO to LUMO singlet transition is located at 343 nm and correlates with the 363 nm band in the absorption spectrum of **4**. The intense absorption band at 273 nm for **4** (in CH_2Cl_2) may be initially assigned to the calculated transition around 293 nm which is an admixture of 60 → 63 and 61 → 63 transitions, namely $d_{x^2-y^2}$(Re) → π*(diimine) and d_{yz}(Re) → π*(diimine) accompanied by partial d(Re) → p_z(carbene C) character. However, the extinction coefficient for this band (1.54×10^4 dm^3 mol^{-1} cm^{-1}) is much larger than that for commonly observed MLCT transitions in rhenium(I) diimine complexes.[24] Furthermore, free bpy shows an intraligand $\pi \rightarrow \pi^*$ transition at 282 nm with ϵ_{max} of 1.48×10^4 dm^3 mol^{-1} cm^{-1}.[25] Hence, it is apparent that the intense absorption of **4** at 273 nm is dominated by the intraligand $\pi \rightarrow \pi^*$ transition of the diimine ligand, which is consistent with previous work on related systems.[24] It should be noted that the calculated intraligand $\pi \rightarrow \pi^*$ transition for the "simplified 2,2′-bipyridine" ligand [NHCHCHNH] in the optimized model **4m** occurs at 232 nm.

Table 5. Electronic Transition Energy Assignment of Optimized Model Molecule 4m by CIS Calculation

no.	excitation state	λ_{calc}, nm	assignment[a]
1	triplet-A″	433	62 → 63, 57 → 63
2	triplet-A′	404	51 → 63, 61 → 63
3	singlet-A″	343	62 → 63
4	triplet-A′	328	60 → 63
5	singlet-A′	323	60 → 63, 61 → 63
6	singlet-A′	293	60 → 63, 61 → 63
7	triplet-A′	280	62 → 64, 62 → 66, 62 → 82
8	triplet-A″	276	60 → 64, 60 → 66, 60 → 70, 60 → 82
9	triplet-A″	270	62 → 63, 56 → 63, 57 → 63
10	singlet-A″	248	61 → 64, 61 → 66
11	singlet-A′	245	62 → 64, 61 → 68, 62 → 66
12	singlet-A″	236	60 → 64, 60 → 66, 60 → 82
13	singlet-A″	232	57 → 63, 62 → 63, 56 → 63
14	singlet-A″	227	61 → 66, 61 → 64, 60 → 82

[a] For the orbitals see Table 3.

The singlet transition energy from HOMO to LUMO (^{1}MLCT), which is assigned to the 363 nm band for complex **4**, is affected by the electronic properties of the 4,4′-substituents on bpy. The LUMO is composed mainly of π*(diimine) (*vide supra*), so electron-donating substituents such as CH_3O and ^{t}Bu will destabilize the LUMO while electron-withdrawing groups such as Cl and CO_2Me will lower the LUMO energy. Thus, a correlation between the ^{1}MLCT transition energy and the Hammett parameters (σ) of the substituents on bpy is anticipated and subsequently demonstrated (see Supporting Information). The ^{1}MLCT transitions of

(23) Foresman, J. B.; Head-Gorden, M.; Pople, J. A.; Frisch, M. J. *J. Phys. Chem.* **1992**, *96*, 135.

(24) (a) Lees, A. J. *Chem. Rev.* **1987**, *87*, 711. (b) Sacksteder, L.; Zipp, A. P.; Brown, E. A.; Streich, J.; Demas, J. N.; DeGraff, B. A. *Inorg. Chem.* **1990**, *29*, 4335. (c) Zipp, A. P.; Sacksteder, L.; Streich, J.; Cook, A.; Demas, J. N.; DeGraff, B. A. *Inorg. Chem.* **1993**, *32*, 5629. (d) Leasure, R. M.; Sacksteder, L.; Nesselrodt, D.; Reitz, G. A.; Demas, J. N.; DeGraff, B. A. *Inorg. Chem.* **1991**, *30*, 3722.

Table 6. Corrected Emission Maxima, Quantum Yields, and Lifetimes for Complexes 2−7 in Dichloromethane and Acetonitrile at Room Temperature

	CH_2Cl_2			CH_3CN		
complex	λ_{max}, nm[a]	ϕ_{em}[b]	τ, ns[b]	λ_{max}, nm[a]	ϕ_{em}[b]	τ, ns[b]
2	558	0.040	194	570	0.012	64
3	553	0.088	330	565	0.038	150
4	565	0.068	230	577	0.021	97
5	603	0.0075	45	615	0.0020	20
6	620	0.015	97	635	0.0039	40
7	555	0.30	2520	565	0.11	932

[a] Error = ±2 nm. [b] Error = ±10%.

2−**6** (Table 4) red-shift as the electron-withdrawing ability of the substituents increases, and this provides further support for the d(Re) → π^*(diimine) (MLCT) assignment of the absorption band.

The MLCT absorption maxima are solvent-dependent and blue-shift *ca*. 10 nm when the solvent is changed from dichloromethane to acetonitrile (Table 4). This solvatochromic effect is a characteristic feature of MLCT transitions. The shift to higher energy in solvents of greater polarity is indicative of a polar ground state and a nonpolar excited state. This is in direct contrast to the effect observed for diimine complexes such as Ru(bpy)$_3^{2+}$ and related systems, where the MLCT band maxima shift to lower energy with increasing solvent polarity typifies a nonpolar ground state and a more polar excited state.[26] Similar negative solvatochromic shifts have previously been observed for the charge-transfer-to-dithiolate and charge-transfer-to-diimine absorption bands of platinum(II) dithiolate[27a] and diimine dithiolate[27b] complexes, respectively.

Emission Spectra and Nature of the Excited States. Photoluminescence has been recorded for complexes **2**−**7** in fluid solution and frozen-solvent glasses. The room-temperature emission data are listed in Table 6, while Figure 5 depicts the emission spectra of **4** (top) and **7** (bottom), respectively, in dichloromethane and acetonitrile at room temperature and in 4:1 ethanol/methanol glass at 77 K. In room-temperature fluid solution, the emission bands are broad and unstructured. The emitting excited states are assigned as d_{xz}(Re) → π^*(diimine) with partial d_{xz}(Re) → p_z(carbene C) on the basis of a linear relationship between the emission and ^{1}MLCT absorption energies (see Supporting Information). The relatively long lifetimes indicate that the transitions involved are spin-forbidden.

The emission energy can be tuned by varying the diimine ligand. The 4,4′-substituents X on the bpy chromophore are expected to strongly affect the MLCT excited-state energy. The carbene complexes with electron-donating substituents on bpy should, therefore, have a greater energy gap between the excited and ground states than those with electron-withdrawing substituents. Hence, a linear correlation between the emission energy and Hammett parameter for X is observed (Figure 6). The shift of the emission band to lower energies for more electron-withdrawing substituents X further supports the assignment of a charge-transfer-to-diimine emitting state. Emission energies are observed to be solvent-dependent, and this is characteristic of MLCT excited states. Emission energies recorded in acetonitrile are red-shifted by *ca*. 400 cm^{-1} compared to those in dichloromethane.

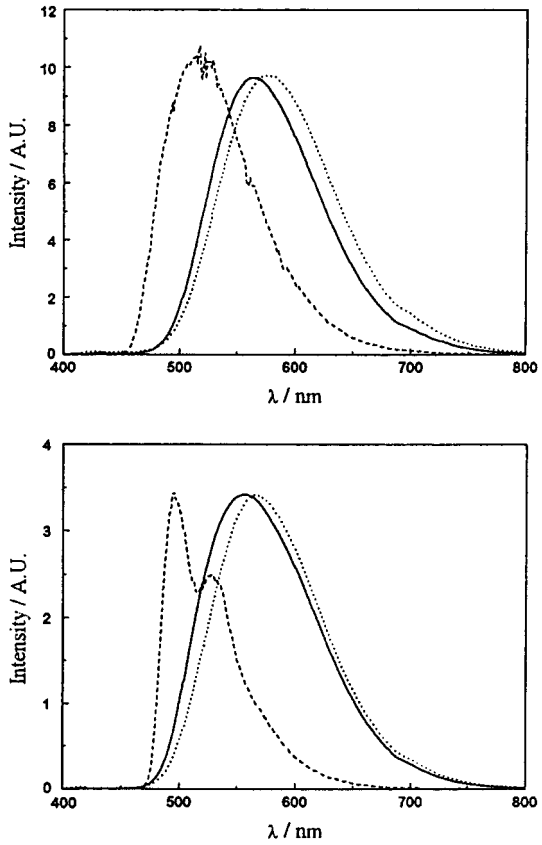

Figure 5. (top) Emission spectra of **4** in dichloromethane (—, λ_{ex} = 365 nm) and acetonitrile (···, λ_{ex} = 355 nm) at room temperature and in 4:1 ethanol/methanol glass (- - -, λ_{ex} = 350 nm) at 77 K. The emission intensities are normalized. (bottom) Emission spectra of **7** in dichloromethane (—, λ_{ex} = 370 nm) and acetonitrile (···, λ_{ex} = 370 nm) at room temperature and in 4:1 ethanol/methanol glass (- - -, λ_{ex} = 350 nm) at 77 K. The emission intensities are normalized.

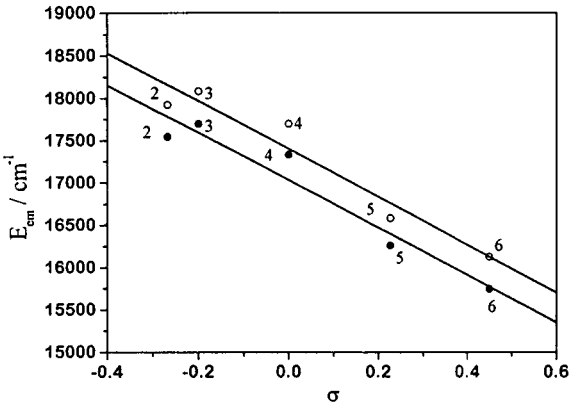

Figure 6. Room-temperature emission energies vs Hammett parameters correlation plots. Complexes are numbered as indicated in Scheme 1. Open circles indicate data in dichloromethane (correlation coefficient R = 0.97, slope = −(2.8 ± 0.4) × 10^3), and closed circles represent data in acetonitrile (R = 0.97, slope = −(2.8 ± 0.4) × 10^3).

(25) Xue, W. M.; Che, C. M. Unpublished work.
(26) Ford, W. E.; Calvin, M. *Chem. Phys. Lett.* **1980**, *76*, 105.
(27) (a) Bevilacqua, J. M.; Zuleta, J. A.; Eisenberg, R. *Inorg. Chem.* **1993**, *32*, 3689. (b) Cummings, S. D.; Eisenberg, R. *J. Am. Chem. Soc.* **1996**, *118*, 1949.

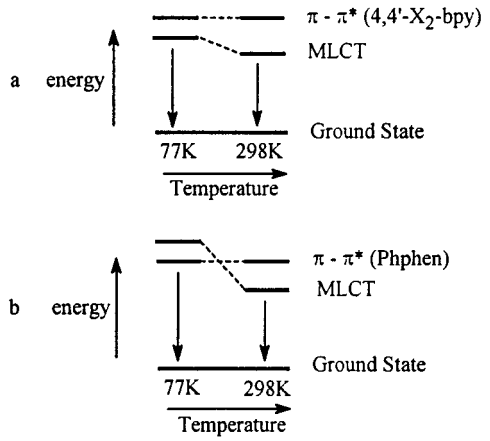

Figure 7. State diagram for the lowest triplet states of (a) $[HNCH_2CH_2NHCRe(4,4'\text{-}X_2\text{-bpy})(CO)_3]^+$ (**2**−**6**) and (b) $[HNCH_2CH_2NHCRe(Phphen)(CO)_3]^+$ (**7**).

The emission spectra of complexes **2**−**6** measured at 77 K in frozen glasses are also broad and virtually structureless, but the emission maxima are shifted to higher energies than at room temperature. However, complex **7** exhibits a structured emission with peaks at 495 and 528 nm in 4:1 ethanol/methanol glass at 77 K. This is clearly phosphorescence of the Phphen ligand (^{3}LC), as indicated by the vibronic structure and its close resemblance to the phosphorescence of the free protonated ligand which has peak maxima at 494 and 522 nm.[24b] Similar emission changes with temperature and ligand had been observed by Zipp, Demas, and DeGraff for rhenium(I) diimine complexes.[24b,c] We adhere to their explanation using the model shown in Figure 7. The 298 and 77 K emissive behavior of **2**−**6** belong to the model in Figure 7a, where all emissions are MLCT. The polar MLCT state energy depends strongly on the solvent organization, while the less polar IL state energy is relatively insensitive to solvent properties. At room temperature, the complex and environment can relax to the thermally equilibrated excited state in a shorter time than the emission lifetime, and this significantly lowers the MLCT state energy. However, in a rigid 77 K glass, solvent viscosity prevents thermal equilibration in a time comparable to the emission lifetime. On the other hand, the emissions of **7** can be represented by the model in Figure 7b. In this case, the emission is MLCT at 298 K but the increase in the MLCT state energy upon cooling means that the MLCT−IL state gap is smaller, and the lowest excited state is IL at 77 K. Apart from the Re(I) derivatives mentioned above,[24] the complexity of multiple luminescences has been encountered for the α-diimine complexes of a number of transition metals, including Ir(III),[28] Cu(I),[29] W(0), and Mo(0).[30] Complex **8**, bearing the phosphine ligand pdpp instead of diimine, does not emit at room temperature in the solution or solid state, but luminescence is observed (λ_{max} 460 nm) in a frozen CH_2Cl_2 solution at 77 K (see Supporting Information). This emission is independent of the excitation wavelength and is assigned to the pdpp IL transition.

Table 7. Electrochemical Data and Excited-State Redox Potentials of Complexes 2−7 in Acetonitrile

complex	$E_{1/2,ox}$ (ΔE_p)[a]	$E_{1/2,red}$ (ΔE_p)[a]	E_{max}, eV	$E_{1/2}(2+/+^*)$, V	$E_{1/2}(+^*/0)$, V
2	+1.50 (90)	−1.38 (80)	2.48	−0.98	+1.10
3	+1.56 (70)	−1.36 (70)	2.51	−0.95	+1.15
4	+1.60 (90)	−1.26 (70)	2.41	−0.81	+1.15
5	+1.62 (90)	−1.04 (50)	2.28	−0.66	+1.24
		−1.62[b]			
		−1.73[b]			
6	+1.66 (120)	−0.86 (60)	2.24	−0.58	+1.38
		−1.38 (70)			
7	+1.59 (90)	−1.31 (50)	2.51[c]	−0.92	+1.20
1	+1.52[b]				

[a] Potentials in volts vs SCE, estimated as $^1/_2(E_{pa} + E_{pc})$, where E_{pa} and E_{pc} are the potentials of peak anodic and cathodic current, respectively; $\Delta E_p = E_{pc} - E_{pa}$. [b] Irreversible. [c] E_{0-0}.

Electrochemistry and Excited-State Redox Properties. Cyclic voltammetry is used to determine the ground-state redox potentials for complexes **2**−**7** (Table 7). A quasireversible oxidation wave in the +1.50 to +1.66 V range (vs SCE) is recorded, which becomes irreversible when the scan speed is decreased from 500 to 100 mV s^{-1}. This couple is assigned to a metal-centered oxidation, i.e., Re(I) → Re(II).[31] One or more reduction waves are observed between −0.86 and −1.73 V, the first of which is reversible while the second and third are irreversible or quasireversible. With reference to electrochemical studies on related rhenium(I) derivatives,[24b,31,32] this first couple is assigned to a ligand-centered $L-L^{0/-}$ reduction.

Both of the ground-state redox potentials $E_{1/2}(Re^{2+/+})$ and $E_{1/2}(L-L^{0/-})$ are systematically varied with different diimine ligands. The plots of $E_{1/2}(Re^{2+/+})$ and $E_{1/2}(L-L^{0/-})$ of complexes **2**−**6** vs the Hammett parameters of the 4,4′-substituents give linear correlations (see Supporting Information). Since the substituents on bpy are not expected to affect the HOMO, which is predominantly comprised of the Re 5d orbital, the variation of oxidation potential $E_{1/2}(Re^{2+/+})$ vs σ is less notable compared to that for $E_{1/2}(L-L^{0/-})$ (slope 0.19 ± 0.03 cf. 0.74 ± 0.05 V, respectively).

A comparison of the electrochemical and emission data gives additional support for the assignment of the Re → π^*(diimine) charge-transfer excited state. A linear relationship is observed between the energy of the excited state and the difference between the ground-state oxidation and reduction potentials (see Supporting Information). Similar correlations have been reported for a number of transition-metal diimine complexes.[27b,32,33]

(28) (a) Watts, R. J.; Brown, M. J.; Griffith, B. G.; Harrington, J. S. *J. Am. Chem. Soc.* **1975**, *97*, 6029. (b) Watts, R. J.; Griffith, B. G.; Harrington, J. S. *J. Am. Chem. Soc.* **1976**, *98*, 674.

(29) (a) Buckner, M. T.; Matthews, T. G.; Lytle, F. E.; McMillin, D. R. *J. Am. Chem. Soc.* **1979**, *101*, 5846. (b) Rader, R. A.; McMillin, D. R.; Buckner, M. T.; Matthews, T. G.; Casadonte, D. J.; Lengel, R. K.; Whittaker, S. B.; Darmon, L. M.; Lytle, F. E. *J. Am. Chem. Soc.* **1981**, *103*, 5906. (c) Casadonte, D. J., Jr.; McMillin, D. R. *J. Am. Chem. Soc.* **1987**, *109*, 331.

(30) (a) Manuta, D. M.; Lees, A. J. *Inorg. Chem.* **1983**, *22*, 572. (b) Manuta, D. M.; Lees, A. J. *Inorg. Chem.* **1986**, *25*, 1354.

(31) Wallace, L.; Rillema, D. P. *Inorg. Chem.* **1993**, *32*, 3836.

(32) Juris, A.; Campagna, S.; Bidd, I.; Lehn, J. M.; Ziessel, R. *Inorg. Chem.* **1988**, *27*, 4007.

(33) (a) Hino, J. K.; Ciana, L. D.; Dressick, W. J.; Sullivan, B. P. *Inorg. Chem.* **1992**, *31*, 1072. (b) Juris, A.; Balzani, V.; Barigelletti, F.; Campagna, S.; Belser, P.; Von Zelewsky, A. *Coord. Chem. Rev.* **1988**, *84*, 85. (c) Rillema, D. P.; Allen, G.; Meyer, T. J.; Conrad, D. *Inorg. Chem.* **1983**, *22*, 1617. (d) Caspar, J. V.; Meyer, T. J. *Inorg. Chem.* **1983**, *22*, 2444. (e) Rezvani, A. R.; Crutchley, R. J. *Inorg. Chem.* **1994**, *33*, 170.

It is also possible to estimate the excited-state redox potentials using the following equations:

$$E_{1/2}(2+/+^*) = E_{1/2}(2+/+) - E_{max} \quad (1)$$

$$E_{1/2}(+^*/0) = E_{1/2}(+/0) + E_{max} \quad (2)$$

where $E_{1/2}(2+/+^*)$ and $E_{1/2}(+^*/0)$ refer to the following reactions, respectively:

$$[(\text{carbene})\text{Re}^{II}(\text{L}-\text{L})^{-}(\text{CO})_3]^{+}{}^* \rightarrow [(\text{carbene})\text{Re}^{II}(\text{L}-\text{L})(\text{CO})_3]^{2+} + e^{-} \quad (3)$$

$$[(\text{carbene})\text{Re}^{II}(\text{L}-\text{L})^{-}(\text{CO})_3]^{+}{}^* + e^{-} \rightarrow [(\text{carbene})\text{Re}^{I}(\text{L}-\text{L})^{-}(\text{CO})_3] \quad (4)$$

Due to the broad structureless nature of the 77 K emissive bands for complexes **2**−**6**, their E_{0-0} values are difficult to determine and, therefore, their respective emission maxima at 77 K in 4:1 ethanol−methanol glass are used as approximations for E_{0-0}. In the case of complex **7**, vibronic structure is observed in the 77 K emission, thus the highest energy vibrational peak is taken as E_{0-0}. It is also important to note that any effects arising from differences in the solvent used for the electrochemical and spectroscopic experiments are not taken into account. Due to these factors, only the relative trends in the calculated excited-state redox potentials should be considered. The results of the calculations are presented in Table 7. The redox potentials for excited states acting as reducing agents, $E_{1/2}(2+/+^*)$, varies from −0.98 V for **2** to −0.58 V for **6**. This reflects the tendency for the ground-state oxidation potentials $E_{1/2,ox}$ to increase and the E_{0-0} values to decrease as the electron-accepting ability of diimine ligands increases. Variations for $E_{1/2}(+^*/0)$ are less significant because both the ground-state reduction potential and E_{0-0} decrease as the 4,4′-substituted bpy becomes more electron-withdrawing. The changes in the excited-state redox potentials for the series generally correlate with the respective Hammett parameters (see Supporting Information). In this investigation, the excited state of complex **2** containing 4,4′-$(MeO)_2$-bpy is the most powerful reductant ($E_{1/2}(2+/+^*) = -0.98$ V) while the excited state of **6** bearing 4,4′-$(CO_2Me)_2$-bpy is the strongest oxidant ($E_{1/2}(+^*/0) = +1.20$ V).

Conclusion

A series of luminescent rhenium(I) complexes of the type $[\overline{\text{HNCH}_2\text{CH}_2\text{NHC}}\text{Re}(\text{L}-\text{L})(\text{CO})_3]^{+}$ (L−L = diimine and diphosphine) have been prepared and characterized by X-ray analysis. Assignment of their lowest-lying excited states is established by investigating their emissive properties at room temperature and 77 K and by interpretation of molecular-orbital calculations. At room temperature, the excited state of complexes **2**−**7** with diimine ligands is assigned as being metal−ligand charge-transfer (MLCT) in nature and is proposed to be predominantly d(Re) → π^*(diimine) with partial d(Re) → σ^*(carbene C). At 77 K, the emitting state of complexes **2**−**6** remains MLCT but that of **7** bearing the Phphen ligand changes to intraligand (IL). Complex **8** with the pdpp ligand does not emit at room temperature, but at 77 K the pdpp IL emission is observed. Excited- and ground-state redox potentials, excited-state energies, emission lifetimes, and quantum yields can be tuned by changing the electron-donating/accepting ability of the auxiliary diimine ligand.

Acknowledgment. We thank The University of Hong Kong, the Croucher Foundation, and the Hong Kong Research Grants Council for financial support. M.C.-W.C. is grateful for a University Postdoctoral Fellowship from The University of Hong Kong. We are indebted to one of the reviewers for helpful suggestions.

Supporting Information Available: ORTEP diagram of **4**, HOMO and LUMO of **4m**, absorption energy vs Hammett parameter plots, emission energy vs ^{1}MLCT absorption energy plots, emission spectrum of **8**, ground state redox potential vs Hammett parameter plot, correlation of emission energies with $\Delta E_{1/2}$, and excited state redox potential vs Hammett parameter plots and tables of crystal data, atomic coordinates, calculated hydrogen coordinates, anisotropic displacement parameters, and bond distances and angles for **4**, **6**, and **8** (36 pages). Ordering information is given on any current masthead page.

OM9709042